Bioelectrochemistry 122 (2018) 191–198

Contents lists available at ScienceDirect

Bioelectrochemistry

journal homepage: www.elsevier.com/locate/bioelechem

Development of an adaptive electroporation system for intratumoral plasmid DNA delivery

Douglas W. Brown [1], Arya J. Bahrami [2], David A. Canton, Anandaroop Mukhopadhyay, Jean S. Campbell [3], Robert H. Pierce [3], Richard J. Connolly [*,3]

OncoSec Medical Incorporated, 5820 Nancy Ridge Drive, San Diego, CA, USA

ARTICLE INFO

Article history:
Received 16 December 2017
Received in revised form 24 March 2018
Accepted 6 April 2018
Available online 09 April 2018

Keywords:
Electroporation
Adaptive electroporation
Gene therapy
Intratumoral therapy
Control systems

ABSTRACT

Intratumoral electroporation of plasmid DNA encoding the proinflammatory cytokine interleukin 12 promotes innate and adaptive immune responses correlating with anti-tumor effects. Clinical electroporation conditions are fixed parameters optimized in preclinical tumors, which consist of cells implanted into skin. These conditions have little translatability to clinically relevant tumors, as implanted models cannot capture the heterogeneity encountered in genetically engineered mouse models or clinical tumors. Variables affecting treatment outcome include tumor size, degree of vascularization, fibrosis, and necrosis, which can result in suboptimal gene transfer and variable therapeutic outcomes. To address this, a feedback controlled electroporation generator was developed, which is capable of assessing the electrochemical properties of tissue in real time. Determination of these properties is accomplished by impedance spectroscopy and equivalent circuit model parameter estimation. Model parameters that estimate electrical properties of cell membranes are used to adjust electroporation parameters for each applied pulse. Studies performed in syngeneic colon carcinoma tumors (MC38) and spontaneous mammary tumors (MMTV-PyVT) demonstrated feedback-based electroporation is capable of achieving maximum expression of reporter genes with significantly less variability and applied energy. These findings represent an advancement to the practice of gene electro-transfer, as reducing variability and retaining transfected cell viability is paramount to treatment success.

1. Introduction

Electroporation (EP) is a process used to deliver membrane-impermeant molecules to cells through the application of pulsed electric fields. It is hypothesized that increased permeability is the result of dielectric breakdown of cell membranes. This phenomenon is observed when the transmembrane voltage is raised above a threshold reported between 200 mV and 1 V (Kinosita and [16,19]). Traditionally, EP parameters are optimized through iterative experiments that investigate the effects of electric field strength, pulse duration, and number of applied pulses on the delivery of exogenous molecules [10,11,15,18]. As tissue heterogeneity affects the distribution of electric fields [7], we hypothesize that fixed EP parameters, optimized in relatively homogeneous tumors, can result in suboptimal gene transfer, when treating tumors in the clinical setting.

A potential solution for suboptimal gene transfer caused by fixed EP parameters is characterization of tissues using electrochemical impedance spectroscopy (EIS). This technique measures electrical responses of a tissue over a range of interrogation frequencies. Collected data is then fit to equivalent circuit models to elucidate the electrical properties of the tissue. Early EIS experiments focused on developing models for single cell characterization. A model commonly used for this purpose is shown in Fig. 1A. This circuit models the intra- and extracellular environment as resistive elements, R_I and R_E respectively, and the cell membrane as a capacitive element, C_M [6].

Advances in EIS techniques have shown complex multicellular environments, such as tissues, can be effectively modeled with an array of interconnected electrical circuits that correspond to individual cells. These advanced models substitute the capacitive membrane element, used in single cell models, with a constant phase element (CPE) that accounts for the spatial distribution of electrical elements [12]. A CPE model commonly used to represent tissue is shown in Fig. 1B. Parameters associated with the CPE element are Q_M and α. The CPE parameter

* Corresponding author at: 1100 Fairview Ave. N., D3-211, Seattle, WA 98109, United States.
E-mail addresses: doug@yourdoug.com, (D.W. Brown), aryab06@gmail.com, (A.J. Bahrami), dcanton@oncosec.com, (D.A. Canton), anand@oncosec.com, (A. Mukhopadhyay), jscampbe@fredhutch.org, (J.S. Campbell), rpierce@fredhutch.org, (R.H. Pierce), rconnoll@fredhutch.org. (R.J. Connolly).
[1] Present Address: Medtronic, 710 Medtronic Parkway, Minneapolis, MN 55432, USA.
[2] Present Address: NanoString Technologies, 530 Fairview Ave. N., Seattle, WA 98109, USA.
[3] Present Address: Fred Hutchinson Cancer Research Center, 1100 Fairview Ave. N., Seattle, WA 98109, USA.

https://doi.org/10.1016/j.bioelechem.2018.04.005
1567-5394/

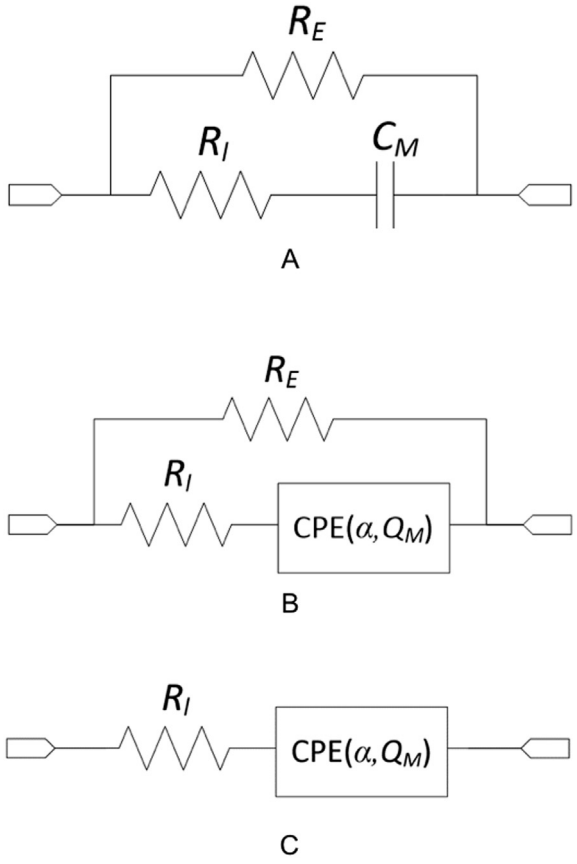

Fig. 1. Circuit models used to represent cells and tissues. (A) Equivalent circuit model for representing a single cell in suspension, (B) CPE model used to represent tissue, and (C) a simplified CPE model used to represent tissue.

Q_M is the charge storage capacity of cell membranes throughout the network equivalent circuits and has units of (farads) × (sec)$^{\alpha-1}$, where the parameter α is a dimensionless quantity that takes on a value between 0 and 1. The CPE circuit model can be represented in the time-domain as:

$$i_M(t) = Q_M \frac{d^{\alpha}}{dt^{\alpha}}[v_m(t)], \tag{1}$$

where $i_M(t)$ is the CPE current in units of A, $v_m(t)$ is the CPE voltage in units of V, t is time in units of s, and d^{α}/dt^{α} is the fractional-order derivative of order α.

The evolution of EIS-based parameters before and after the application of EP pulses has been shown to improve both diagnostic and gene delivery approaches. An EIS-based technique was first used as a diagnostic metric for monitoring irreversible EP in rat liver [8,14]. In addition, EIS has been used to distinguish between reversible and irreversible EP in murine fibrosarcomas *in vivo* [13]. Studies performed on *ex vivo* lung and tumor tissue showed impedance changes are measureable following EP, indicating electrical changes may be used as an indicator of successful EP [3,17]. Recently, changes in the magnitude of impedance have been used as a control parameter for stopping the EP process to improve the delivery of plasmid DNA in skin [1]. These studies provide fundamental evidence that EIS can be used to control and assess EP, but still rely on conditions optimized in homogeneous tissues.

Development of equivalent circuit models capable of accurately fitting a range of tissues, irrespective of heterogeneity, is critical to the development of a highly-controlled EP system. The ability to estimate bulk tissue properties during treatment enables EP pulse durations to be set in real time using a multiplier of the bulk tissue time constant. As charge saturation from an applied electric field occurs in capacitive elements when five or more multiples of the equivalent circuit time constant is applied, it was assumed this would result in a higher degree of transfection. For the CPE-based equivalent circuit model in Fig. 1B the impedance, Z in units of ohms, has been shown to be

$$Z(j2\pi f) = \frac{R_I R_E}{R_I + R_E} + \frac{R_E - \frac{R_I R_E}{R_I + R_E}}{1 + \left[j2\pi f[(R_I + R_E)Q_M]^{\frac{1}{\alpha}}\right]^{\alpha}} \tag{2}$$

where f is frequency in Hz and $j = \sqrt{-1}$ is a dimensionless constant [12]. In tissues the observed resistance of the intracellular environment is orders of magnitude less than the resistance of the extracellular environment allowing for the approximation $R_E \gg R_I$ of Eq. (2) and simplifying to arrive at,

$$Z{\sim}(j2\pi f) = \lim_{R_I/R_E \to 0} Z(j2\pi f) = R_I + \frac{1}{Q_M[j2\pi f]^{\alpha}}. \tag{3}$$

The corresponding circuit representation for $Z{\sim}$ can be realized as the simplified model in Fig. 1C. The expression for $Z{\sim}$ in Eq. 2 can be rewritten as,

$$Z{\sim}(j2\pi f) = \frac{1 + \left[j2\pi f(R_I Q_M)^{1/\alpha}\right]^{\alpha}}{Q_M(j2\pi f)^{\alpha}}. \tag{4}$$

The 3 dB cutoff frequency $f_{3\mathrm{dB}}$ associated with the numerator of Eq. 4 can be computed by solving $|[2\pi f_{3\mathrm{dB}}(R_I Q_M)^{1/\alpha}]^{\alpha}| = 1$. This allows the bulk tissue time constant, τ, to be computed as,

$$\tau = (R_I Q_M)^{1/\alpha}. \tag{5}$$

Comparison of impedance magnitude for a CPE model and simplified CPE model showing the relative locations of R_E, R_I, and $f_{3\mathrm{dB}}$ is provided in Fig. 2. This model was generated using $R_E = 20\mathrm{k}\Omega$, $R_I = 500\Omega$, $Q_M = 10^{-5}\,\mathrm{Fs}^{-0.3}$, and $\alpha = 0.7$. The relative 3 dB frequency and corresponding bulk tissue time constant can be computed as $f_{3\mathrm{dB}} = 1.94$ kHz and 516 μs, respectively. Finally, q_M represents the total charge applied across cell membranes, in units of C, when an EP pulse is applied for $t > 0$. Then $q_{\infty} = \lim_{t \to \infty} q_M$ for the steady-state charge across the collection of cell membranes, or

$$q_M = q_{\infty}(1 - \exp(-t/\tau)). \tag{6}$$

The percent of total charge applied across the cell membranes for $t = 1\tau$, 2τ, 3τ, 5τ, and 10τ corresponds to 63%, 86%, 95%, 99%, and 99.96%, respectively.

To overcome the issues presented by EP optimization routines and tissue heterogeneity, a more fundamental method of developing pulse parameters is required. To test the efficacy of time constant-based EP, or adaptive EP, a custom generator was fabricated. This generator collected real-time EIS data and fit these data to the CPE model shown in Fig. 1C. Pulse durations were adapted based on the calculated time constant and a pre-programmed multiplier. To ascertain the flexibility of this system, two distinctly different tumor models were tested. The first model was a syngeneic tumor consisting of immortalized murine colon carcinoma cells (MC-38), representing a less heterogeneous tumor. The second was a genetically engineered spontaneous mammary tumor model (MMTV-PyVT), representing a more heterogeneous tumor. As depicted in Fig. 3, the MMTV-PyVT tumors are comprised of an admixture of cells with vasculature, focal necrosis, and stroma. In contrast, syngeneic tumors, which are frequently used to determine optimum EP parameters, are more homogenous.

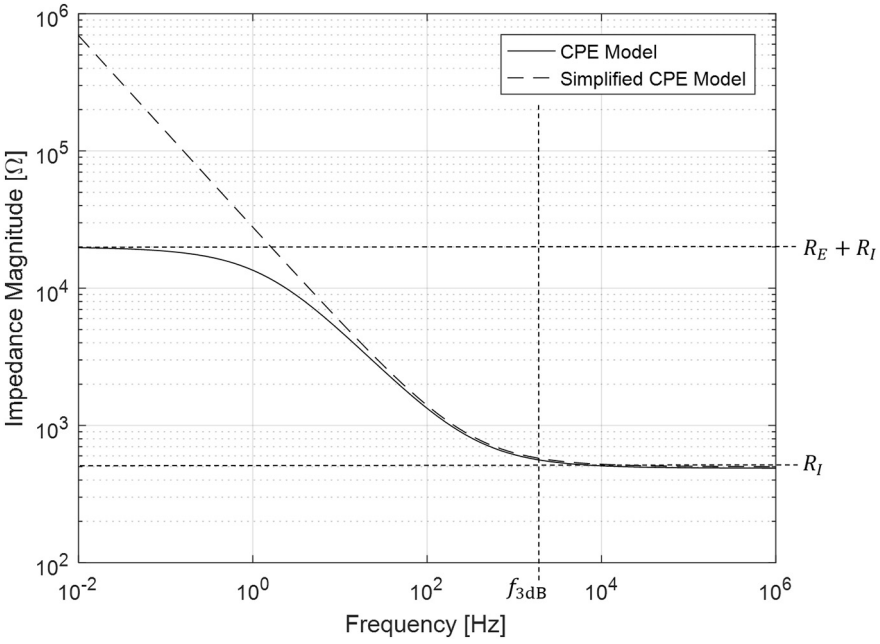

Fig. 2. Comparison of CPE and simplified CPE models. Impedance magnitude for a CPE model (solid line) and simplified CPE model (dashed line) showing the relative locations of R_E, R_I, and f_{3dB}. Models were generated using $R_E = 20$ kΩ, $R_I = 500$ Ω, $Q_M = 10^{-5}$ $Fs^{-0.3}$, and $\alpha = 0.7$.

2. Materials and methods

2.1. EP generator

A custom rectangular-wave EP generator was fabricated (Fig. 4A), that was capable of operating in either open-loop or closed-loop configurations. To determine the efficacy of adaptive EP, the device was operated using a closed-loop configuration, where the estimated time constant of the tissue was used as the control parameter. Time constants were computed from best-fit vector models using frequency, magnitude, and phase data from EIS measurements. Operational constraints were imposed to limit the pulse duration between 100 μs and 10 ms.

A combination of solid-state relays (SSRs) and fast-switching p-type metal-oxide semiconductor field effect transistors (pMOSFET) were used to switch between the pulse generator and EIS instrumentation. SSRs are effective in isolating high-voltage pulses from sensitive instrumentation circuitry. However, SSRs have a response time of 5 ms. Therefore, a pMOSFET was used to control waveform generation with a response time of 500 ns. A 32-bit ARM microcontroller (STM32F407VGT6, STMicroelectronics) was used to control the pulse sequence and perform data acquisition.

2.2. EIS data acquisition

Impedance spectroscopy measurements were acquired using a set of low-pass filters, a digital-to-analog converter (DAC), and two analog-to-digital converters (ADC). A 16-bit DAC (LTC1668, Linear Technology) converted the reference signal generated from the microcontroller into a potential applied across the EP applicator. To eliminate common-mode and high-frequency noise, the applied voltage and response current was measured using a pair of differential instrumentation amplifiers (LT1801, Linear Technology) with a two-stage low-pass filter having an 8th order pole at 2.5 MHz and 2nd order pole at 20 kHz (LT6600-2.5, Linear Technology). The filtered signals were each sampled by a 14-bit successive approximation ADC (LTC1740, Linear Technology).

Measurements were collected for a logarithmically spaced range of sinusoidal signals from 100 Hz to 10 kHz, f_0, with a resolution of 15

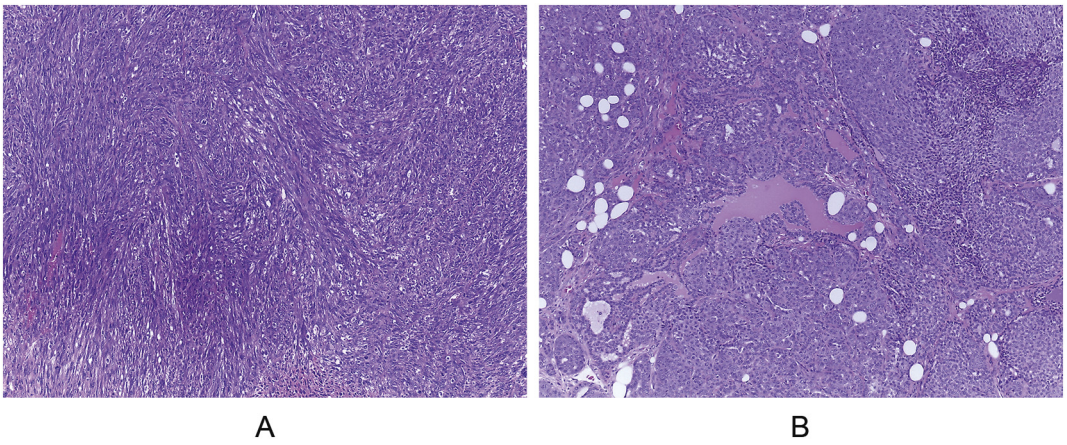

Fig. 3. Heterogeneity of syngeneic and spontaneous tumor models. Histology of (A) MC38 and (B) MMTV-PyVT tumor tissue. Tumor tissue was excised and fixed in 10% neutral buffered formalin. Sections were then stained with hematoxylin and eosin Representative images are shown at 10× magnification.

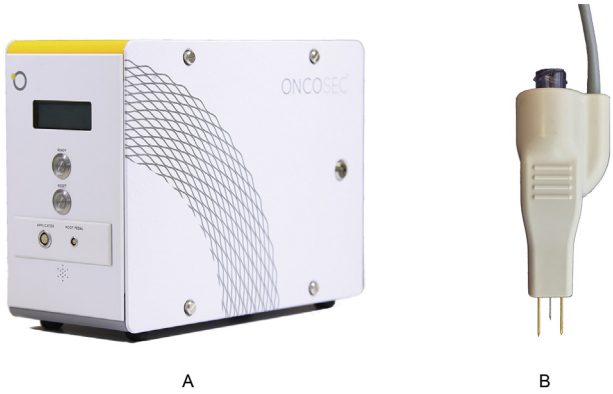

Fig. 4. EP hardware fabricated for studies. (A) Feedback EP generator and (B) applicator used throughout these studies.

samples per decade. During spectra acquisition, an excitation signal was produced by the generator and applied across the EP applicator electrodes. Each excitation signal contained two periods, T_0, of a $1V_{pp}$ sinusoidal waveform. Each waveform was generated using 70 discrete samples with a period of T_s. To achieve this, the waveform sample frequency was dynamically set to $f_s = 35f_0$ resulting in an overall DAC sampling range from 3.5 kHz to 350 kHz. The first period of the excitation signal was used to precondition the charge across the tissue, and the second period of the excitation was measured, as shown in Fig. 5. The applied voltage and resulting current were over-sampled by a factor of ten resulting in an ADC sample frequency of $10f_s$ ranging from 35 kHz to 3.5 MHz, or a factor of 175 times the Nyquist frequency. Data were then averaged and decimated by a factor of 10 to further reduce measurement noise. A set of 35 voltage and current samples corresponding to each frequency were stored locally in the microcontroller's internal random access memory for post-processing. Once data acquisition completed, the current and voltage measurements were used in an extended Kalman filter for optimal estimation and de-noising of the magnitude and phase for a known applied excitation sinusoidal frequency f_0. This was repeated for all 30 frequency points. The resulting spectra are used with a non-linear least-squares regression routine to estimate the model parameters R_I, Q_M, and α from Eq. (3) and compute the time constant from Eq. (5). The final measured spectra and modeling parameters were then stored in non-volatile memory for later analysis.

2.3. EP applicator

To reduce variability associated with co-locating the electric field and plasmid DNA injectate, a custom applicator, shown in Fig. 4B, was developed. The body of this applicator was manufactured with injection molded parts and housed the electrodes, hypodermic needle, and a luer fitting to interface with a standard syringe. Electrodes were trocars having an exposed length of 7 mm and diameter of 0.44 mm. Parallel electrodes were separated by a 5 mm gap. These electrodes were composed of 304 stainless steel and had 2.5 μm of gold electrodeposited onto the surface. This gold coating reduced the effects of electrochemical degradation caused by high voltage EP pulses. A 30-gauge stainless steel hypodermic needle with an exposed length of 5 mm was centered between the trocar electrodes. A luer fitting was placed on the opposite side of these elements to allow a syringe to be paired with the device. Electrical interfacing was performed with a twisted pair of shielded wires built into the applicator. This wire terminated to a circular high density connector that housed an electrically erasable programmable read-only memory (EEPROM) chip. The EEPROM stored information pertaining to the applicator model, serial number, number of uses, and operating parameters for the EP process.

2.4. Syngeneic tumor model

To generate homogeneous tumors for initial device testing, immortalized mouse murine colon adenocarcinoma cells (MC38, gift from Dr. H. Kohrt) were used. These cells were cultured in Dulbecco's Modified Eagle medium containing 10% fetal bovine serum, 2 mM L-glutamine, 0.1 mM nonessential amino acids, 1 mM sodium pyruvate, 10 mM HEPES, 100 U/ml penicillin, 100 μg/ml streptomycin, and 50 μg/ml gentamycin sulfate (Gibco) and incubated at 37 °C in 5% CO_2 and subcultured at 80% confluency.

Six-week-old female B6-albino mice were obtained for implanting syngeneic tumors (Strain: 000058, The Jackson Laboratory). Following a 72-h acclimation period, mice were anesthetized with 2% isoflurane in 500 ml/min oxygen. After induction, 10^6 MC38 cells suspended in 50 μl of Dulbecco's phosphate buffered saline (D-PBS, Gibco) were injected into the subcutaneous tissue on the left and right flanks with a 27-gauge syringe. Tumor volumes were monitored by two-dimensional caliper measurements [4] until the volume reached approximately 100 mm^3, which coincided with 10 days post injection.

2.4.1. Syngeneic tumor experimental design

MC38 tumor were treated when volumes reached 100 $mm^3 \pm 20\%$. Treatment was performed by placing the integrated applicator perpendicularly into the longer tumor axis. Each element was inserted until the injection lumen reached the center of the tumor. After insertion tumors were injected with 50 μl of a 1 mg/ml solution of plasmid DNA suspended in physiological saline. The plasmid used in these experiments encoded luciferase and mCherry proteins linked by a P2A ribosomal skipping motif (Luc2P-P2A-mCherry) and under control of a CMV promoter. After injection, adaptive EP was initiated, where EIS

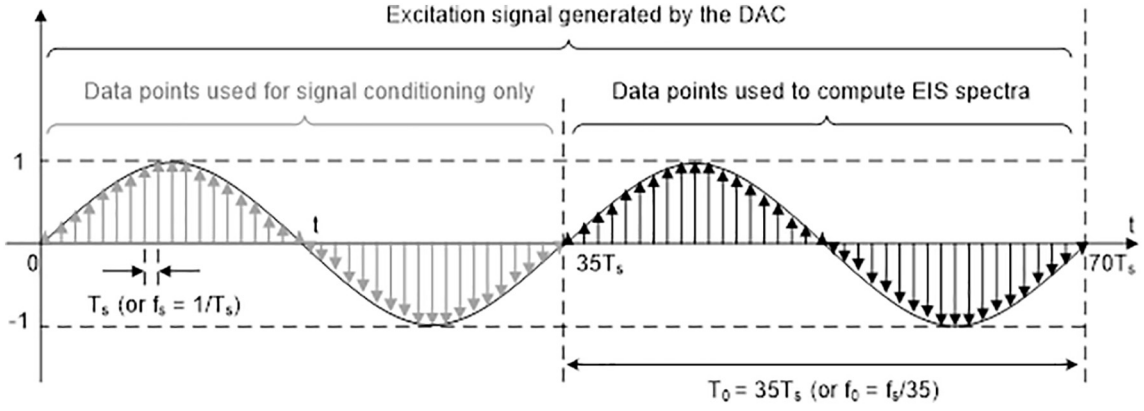

Fig. 5. Excitation signal generated by the DAC. Plot showing the excitation signal generated by the digital-to-analog controller. This plot illustrates the sampling rate and data used to compute EIS spectra.

data was acquired and fit to the CPE model prior to each pulse. An estimate of the bulk tissue time constant was determined by Eq. (5). The duration of each EP pulse was defined by a multiple of the tissue time constant, where multiples of 0.1, 0.2, 0.5, 2.0, 5.0, 10.0, and 20.0 were used for these experiments. A total of eight pulses were delivered with a nominal electric field magnitude of 400 V/cm. A delay of 300 ms between successive pulses allowed for the collection and computation of EIS, as well as augmentation of pulse parameters. An injection only group served as the control group for this experiment. Ten tumors were treated with each condition in this experiment.

2.5. Spontaneous tumor model

Female transgenic mice expressing the mouse mammary tumor virus (MMTV) long terminal repeat upstream of a cDNA sequence encoding the Polyoma Virus middle T (PyVT) antigen (Strain: 002374, The Jackson Laboratory) were obtained for testing in a heterogeneous tumor. These mice developed palpable mammary tumors at five weeks of age, which were monitored by two-dimensional caliper measurements [5] until their tumor volumes reached approximately 100 mm^3. This occurred at approximately eight weeks of age [2,9].

2.5.1. Spontaneous tumor experimental design

MMTV-PyVT tumor were treated when volumes reached 100 mm^3 ± 20% by two-dimensional caliper measurements. Similarly, treatment was performed by placing the integrated applicator perpendicularly into the larger tumor axis, and the injection lumen was placed in the center of the tumor. Tumors were then injected with 50 μl of a 1 mg/ml solution of plasmid DNA encoding for luciferase and mCherry proteins. After injection, feedback controlled EP was performed, where EIS data was acquired and fit to the CPE model prior to each pulse. Based on results from the MC38 experiments, a multiplier of ten estimated tissue time constants was selected for the EP pulse duration. Again a total of eight pulses were delivered with a nominal electric field magnitude of 400 V/cm and 300 ms delay between successive pulses. This was compared to tumors treated with conditions optimized for these tumors, where eight 10 ms pulses were applied at 400 V/cm. Additionally, an injection only control was performed. A total of 18 tumors were treated with each condition in this experiment.

2.6. Tumor histology

Spontaneous and syngeneic tumors were excised and immediately fixed in 10% neutral buffered formalin. Fixed tissues were processed and sections were stained with hematoxylin and eosin to visualize cellular features. Images were captured on an Aperio ImageScope system (Leica Biosystems).

2.7. In vivo imaging

An *in vivo* imaging system (Lago, Spectral Instruments) was used to quantify luminescence of tumors 48 h after treatment. To perform imaging, animals were placed in an induction chamber and exposed to 2% isoflurane in 500 ml/min of oxygen. Once anesthetized, 200 μl of a 15 mg/ml solution of D-luciferin (Gold Bio) prepared in D-PBS was administered by intraperitoneal injection with a 27-gauge syringe. Animals were then transferred to an anesthesia manifold on a 37 °C heated stage, where they continued to receive 2% isoflurane in 500 ml/min of oxygen. Luminescent images were acquired 20 min after injection using a 5 s exposure to a CCD camera cooled to -90 °C. Total photons emitted from each tumor was determined by post-processing using a region of interest with a 0.5 cm radius (AmiView, Spectral Instruments).

2.8. Statistical methods

Electrical data collected from EIS and EP procedures was stored on internal memory in the generator. After downloading, this data was processed using MATLAB to determine generator performance and tissue properties, such as time constant distribution. Luminescence data gathered from these experiments and analyzed using GraphPad Prism software. Statistical significance was analyzed using a Kruskal-Wallis one-way analysis of variance test with a post-hoc Dunn's test. A significance level of 0.05 was selected for all statistical data analysis.

2.9. Ethics statement

All experiments were performed in accordance with an approved Institutional Care and Use Committee protocol in a vivarium facility (Explora BioLabs) approved by the Association for the Assessment and Accreditation of Laboratory Animal Care International.

3. Results

An intelligent EP system required building a generator with integrated tissue sensing capabilities. Tissue sensing was accomplished with a 32-bit ARM Cortex microcontroller using low-noise amplifiers with instrumentation containing analog-to-digital and digital-to-analog converts with a sampling rate of 2.5 MHz. Prior to each EP pulse, EIS data was automatically collected by actuating a bank of solid-state relays that separated the pulsing circuit and tissue sensing circuit. Data were collected from 100 Hz to 10 kHz at a resolution of 15 points per decade using a 1 V excitation signal and measuring current responses.

Capturing electrochemical responses over the defined frequency range and adjusting EP parameters required a total of 300 ms. This included 100 ms for raw signal generation and sampling, 75 ms for on-board data processing, and 125 ms to ensure proper actuation of solid-state relays between each EP pulse. Once collected, raw data were preprocessed to remove signal offsets before being passed through a linear quadratic estimation algorithm, specifically an extended Kalman filter, to estimate the magnitude and phase response at each frequency. After filtering, data were fit to one of four models (resistive, capacitive, CPE, and unknown) using a model selection routine based on the coefficient of determination computed for each respective model. The resistive model was used to identify short circuit conditions before applying each EP sequence. The capacitive model was used to identify when electrodes were not in contact with tissue prior to EP. The CPE model verified the presence of tissue before and after EP and was used to compute the optimum EP pulse width. Finally, if any of the three models did not have a coefficient of determination >0.98, the model was considered unknown and open-loop or traditional EP conditions were applied by default. Fig. 6 demonstrates a sample set of EIS data and the correlating fit to the CPE equivalent circuit model. During the course of these experiments, the modeling routine did not select the CPE model in 0.35% of all EP pulses. Tumor EIS data not fitting the CPE model were removed from the study.

By fitting EIS data to the CPE equivalent circuit model, using Eq. (5) and depicted in Fig. 6, a time constant could be quantified prior to delivery of each EP pulse. Time constants computed for MC38 tumors followed a normal distribution with an average computed time constant of 161 μs and a standard deviation of 54 μs (Fig. 7A). Computed time constants for MMTV-PyVT tumors followed a log-normal distribution with an average of 279 μs and a standard deviation of 164 μs (Fig. 7B). The difference in distribution of time constants observed for MC38 and MMTV-PyVT tumors indicates that EIS and CPE modeling are able to distinguish between two types of tumor heterogeneity.

To determine the efficacy of adaptive EP on delivery of plasmid DNA in homogeneous tumor tissues, MC38 tumors were injected with 50 μg of a plasmid encoding luciferase. After injection, the EP process was

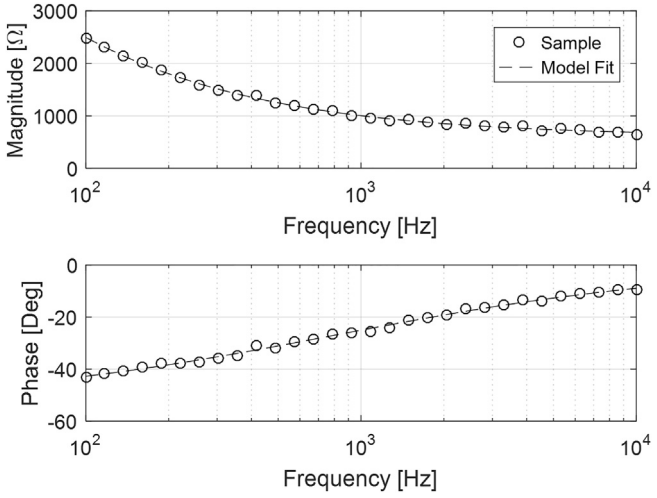

Fig. 6. Fit of EIS data to simplified CPE model. EIS magnitude (A) and phase data (B) collected by tissue sensing circuitry in the adaptive EP generator. Raw magnitude and phase data (circles) is shown with a corresponding simplified CPE equivalent circuit model fit (solid line).

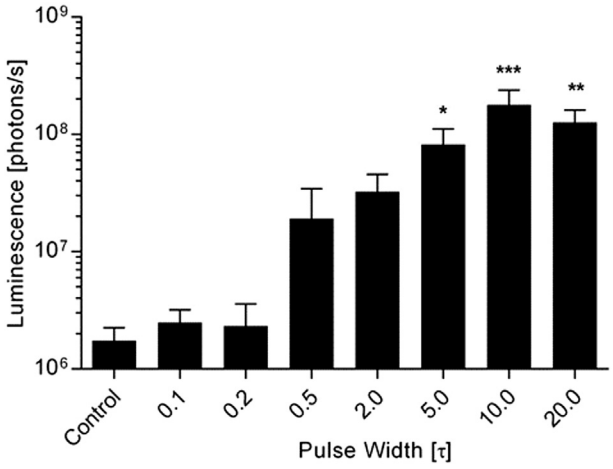

Fig. 8. Reporter expression at tested adaptive EP pulse widths. Mean luminescence observed in MC-38 tumors 48 h after EP applied with a predefined multiple of the computed time constant. Error bars indicate standard error of the mean. Significant increases in mean were observed for pulse widths greater than 5τ, where * indicates $p < 0.05$, ** indicates $p < 0.01$, and *** indicates $p < 0.001$.

initiated on the generator using the integrated applicator. Each pulse in a series of eight was performed using pre-programmed multiples of the time constant computed from the CPE model fit. Specifically, EP sequences were applied at 0.1, 0.2, 0.5, 2.0, 5.0, 10.0, and 20.0 multiples of the computed time constant. Luminescence data was acquired at 48 h with an *in vivo* imaging system following intraperitoneal injection of 3 mg D-luciferin. A rise in mean luminescence of 1.5-fold over injection alone was found for 0.1, 1.3-fold for 0.2, 11.0-fold for 0.5, 18.6-fold for 2.0, 47.3-fold for 5.0, 102.6-fold for 10.0, and 72.8-fold for 20.0 multiples of the computed time constant. Only EP conditions performed at 5.0 multiples of the computed time constant and higher resulted in statistically significant rises in mean luminescence compared to injection of plasmid DNA only. These higher time constant groups, however, were not significantly different from each other at a significance level of 0.05. Fig. 8 shows the observed 48-h luminescence at each EP condition tested.

To ascertain the ability of adaptive EP to deliver plasmid DNA to heterogeneous tumor tissue, spontaneous MMTV-PyVT tumors were treated. These tumors were first injected with 50 μg of a plasmid encoding luciferase and then treated with either adaptive or fixed duration EP. Based on the performance observed in MC-38 tissue and the proposed mechanism requiring complete charge saturation of membranes, 10 multiples of the computed time constant was selected as the optimum adaptive EP pulse duration. This was compared to fixed duration EP conditions that had been optimized through an iterative process for MMTV-PyVT tumors. Peak luminescence data is presented using a box-and-whisker plot in Fig. 9. A rise in mean luminescence of 376-fold for fixed conditions and 913-fold for adaptive conditions was observed when these groups were compared to injection only control. Analysis of these data show a statistically significant rise in luminescence when adaptive and fixed EP groups are compared to injection only control ($p < 0.001$). However, direct comparison of mean luminescence in the adaptive and fixed EP groups showed no statistical difference when analyzed at a significance level of 0.05. An F-test comparing the variance in luminescence of the two EP groups in Fig. 9 shows the group treated with adaptive EP have significantly smaller variance than traditional EP ($p < 0.01$). A post-hoc analysis of generator performance data was carried out in MATLAB to determine the total

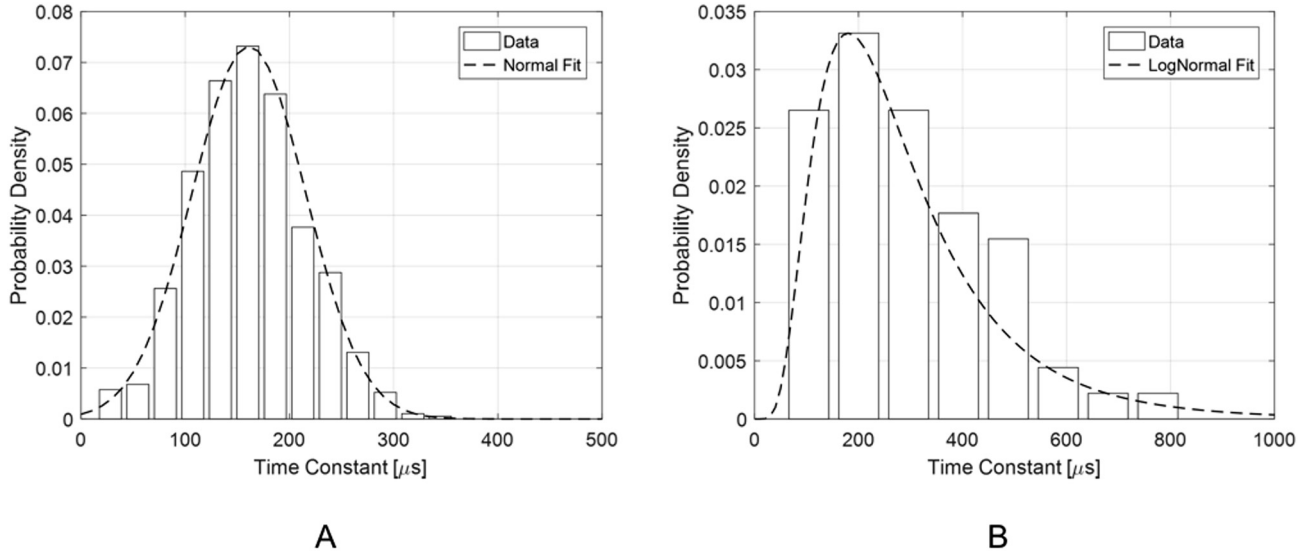

Fig. 7. Distribution of time constants in syngeneic and spontaneous tumor models. (A) Probability density of time constants observed for MC-38 tumors with an overlay of a normal fit. (B) Time constant probability density of MMTV-PyVT tumors with an overlay of a log-normal fit.

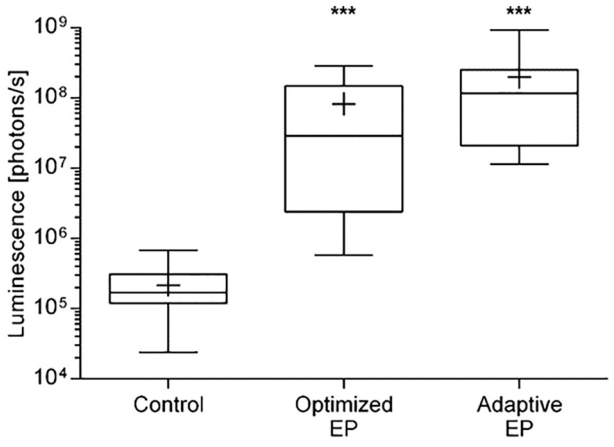

Fig. 9. Reduction in expression variance with adaptive EP. Box-and-whisker plot showing the variance of luminescence data obtained by injection only, optimized EP, and adaptive EP. The line represents the median luminescence, a cross represents the mean of each group, and upper and lower quartiles represent the 95th and 5th percentile, respectively. Adaptive and optimized EP were found to be significant over injection only controls, where *** indicates $p < 0.001$.

energy delivered for with each EP condition. This analysis found fixed EP conditions delivered an average of 1.197 J with a standard deviation of 0.489 J, while the adaptive conditions delivered an average of 0.179 J with a standard deviation of 0.060 J, a difference of approximately 10-fold. These data indicate adaptive conditions deliver significantly less energy than fixed conditions.

4. Discussion

Results obtained in this study provide evidence that equivalent circuit models can be used to control the application of EP. Data gathered in experiments with homogeneous and heterogeneous tumors were fit to the simplified CPE model to adjust parameters when performing adaptive EP. Performing EP with adaptive parameters resulted in similar levels of peak expression as fixed EP, but with significantly less variability and less energy delivered to the tissue. These findings suggest EP parameters can be adjusted in real time for the tissue being treated, while reducing site-to-site variability. Additionally, the application of less energy will likely result in less collateral tissue damage and a longer duration of plasmid DNA expression.

In the course of these experiments, a total of three simplified CPE fit failures resulted in the application of fixed duration pulses. These events occurred in one tumor EP sequence where pulses were delivered at 20 multiples of the computed time constant. The failure to fit the simplified CPE model was likely the result of gold coating degradation on the applicator electrodes. Analysis of data from this EP sequence was removed from the study. Thus, any EIS data that does not fit the CPE model will result in the application of fixed duration pulses that are currently used in the clinic. Therefore, under this worst-case scenario, clinical parameters would be delivered to the tissue.

Delivery of plasmid DNA in homogenous tissues followed the predicted dose-response curve, where significance was achieved at and above five multiples of the computed time constant. This observation provides further evidence to the theory of EP being a dielectric breakdown phenomena. While significant rises in expression over control were observed in this experiment at 5, 10, and 20 multiples of the time constant, it is reasonable to assume extending pulse durations beyond the tested range would result in the irreversible EP and reduce plasmid DNA expression. Each applied pulse duration resulting in membrane charge saturation had a significant rise in expression when compared to control, but were not significantly different from one another. Therefore, a multiple of 10 time constants was selected as the optimum closed-loop condition, as this corresponded to 99.96% charge saturation and had the highest overall mean expression. Delivery of plasmid DNA using adaptive EP was tested in a heterogeneous tumor environment using a spontaneous breast cancer tumor model (MMTV-PyVT). Expression data was compared to injection only and fixed optimized EP conditions. While the overall mean expression levels for EP groups showed no significant difference, the variability associated with tumors treated with adaptive EP was significantly smaller than the observed variability in tumors treated with fixed EP conditions. This is likely the result of the adaptive conditions applying the electric field for a sufficient amount of time to result in delivery, but not over applying the field to result in irreversible tissue damage. This is further supported by the adaptive condition delivering an order of magnitude less energy than traditional or fixed EP conditions.

The implications of basing EP parameters on equivalent circuit models provides a more controllable route of administration than the current state of the art platforms being used clinically. This is observed by the ability to maximize plasmid DNA expression levels and reduce the amount of variability associated with the delivery irrespective of tissue heterogeneity. This improves the likelihood of observing clinically relevant responses when delivering plasmid DNA to tissue, which should progress adoption of this technology as a localized delivery platform. Delivering less energy than fixed duration pulses should result in reduced transient pain and muscle stimulation. Additionally, the application of less energy will likely lead to less collateral tissue damage and should extend the duration of expression. Ultimately the goal of these advancements are to automate the EP process, and therefore not be reliant on optimization routines and user inputs.

Conflict of interest

At the time the described research was conducted all authors were full time employees of OncoSec Medical Incorporated. Additionally, authors on this work are named inventors on intellectual property filings pertaining to the subject matter described.

References

[1] R.M. Atkins, T.J. Fawcett, R. Gilbert, A.M. Hoff, R. Connolly, D.W. Brown, A.J. Llewellyn, M.J. Jaroszeski, Impedance spectroscopy as an indicator for successful in vivo electric field mediated gene delivery in a murine model, Bioelectrochemistry 115 (2017) 33–40.
[2] S.A. Davie, J.E. Maglione, C.K. Manner, D. Young, R.D. Cardiff, C.L. MacLeod, L.G. Ellies, Effects of FVB/NJ and C57Bl/6J strain backgrounds on mammary tumor phenotype in inducible nitric oxide synthase deficient mice, Transgenic Res. 16 (2) (2007) 193–201.
[3] D.A. Dean, T. Ramanathan, D. Machado, R. Sundararajan, Electrical impedance spectroscopy study of biological tissues, J. Electrost. 66 (3–4) (2008) 165–177.
[4] D.M. Euhus, C. Hudd, M.C. LaRegina, F.E. Johnson, Tumor measurement in the nude mouse, J. Surg. Oncol. 31 (4) (1986) 229–234.
[5] A. Faustino-Rocha, P.A. Oliveira, J. Pinho-Oliveira, C. Teixeira-Guedes, R. Soares-Maia, R.G. da Costa, B. Colaco, M.J. Pires, J. Colaco, R. Ferreira, et al., Estimation of rat mammary tumor volume using caliper and ultrasonography measurements, Lab. Anim. (NY) 42 (6) (2013) 217–224.
[6] H. Fricke, S. Morse, The electric resistance and capacity of blood for frequencies between 800 and 4(1/2) million cycles, J. Gen. Physiol. 9 (2) (1925) 153–167.
[7] A. Golberg, B.G. Bruinsma, B.E. Uygun, M.L. Yarmush, Tissue heterogeneity in structure and conductivity contribute to cell survival during irreversible electroporation ablation by "electric field sinks", Sci. Rep. 5 (2015) 8485.
[8] Y. Granot, A. Ivorra, E. Maor, B. Rubinsky, In vivo imaging of irreversible electroporation by means of electrical impedance tomography, Phys. Med. Biol. 54 (16) (2009) 4927–4943.
[9] C.T. Guy, R.D. Cardiff, W.J. Muller, Induction of mammary tumors by expression of polyomavirus middle T oncogene: a transgenic mouse model for metastatic disease, Mol. Cell. Biol. 12 (3) (1992) 954–961.
[10] R. Heller, Y. Cruz, L.C. Heller, R.A. Gilbert, M.J. Jaroszeski, Electrically mediated delivery of plasmid DNA to the skin, using a multielectrode array, Hum. Gene Ther. 21 (3) (2010) 357–362.
[11] R. Heller, M. Jaroszeski, A. Atkin, D. Moradpour, R. Gilbert, J. Wands, C. Nicolau, In vivo gene electroinjection and expression in rat liver, FEBS Lett. 389 (3) (1996) 225–228.
[12] E. Hernandez-Balaguera, E. Lopez-Dolado, J.L. Polo, Obtaining electrical equivalent circuits of biological tissues using the current interruption method, circuit theory and fractional calculus, RSC Adv. 6 (2016) 22312–22319.

[13] A. Ivorra, B. Al-Sakere, B. Rubinsky, L.M. Mir, In vivo electrical conductivity measurements during and after tumor electroporation: conductivity changes reflect the treatment outcome, Phys. Med. Biol. 54 (19) (2009) 5949–5963.
[14] A. Ivorra, B. Rubinsky, In vivo electrical impedance measurements during and after electroporation of rat liver, Bioelectrochemistry 70 (2) (2007) 287–295.
[15] S. Jaichandran, S.T. Yap, A.B. Khoo, L.P. Ho, S.L. Tien, O.L. Kon, In vivo liver electroporation: optimization and demonstration of therapeutic efficacy, Hum. Gene Ther. 17 (3) (2006) 362–375.
[16] K. Kinosita Jr., T.Y. Tsong, Voltage-induced pore formation and hemolysis of human erythrocytes, Biochim. Biophys. Acta 471 (2) (1977) 227–242.
[17] B.J. Mossop, R.C. Barr, J.W. Henshaw, D.A. Zaharoff, F. Yuan, Electric fields in tumors exposed to external voltage sources: implication for electric field-mediated drug and gene delivery, Ann. Biomed. Eng. 34 (10) (2006) 1564–1572.
[18] T. Muramatus, O. Shibata, S. Ryoki, Y. Ohmori, J. Okumura, Foreign gene expression in the mouse testis by localized in vivo gene transfer, Biochem. Biophys. Res. Commun. 233 (1) (1997) 49.
[19] J. Teissie, M.P. Rols, An experimental evaluation of the critical potential difference inducing cell membrane electropermeabilization, Biophys. J. 65 (1) (1993) 409–413.